Grating pseudo-imaging with polychromatic and finite extension sources

Lucas García-Rodríguez, José Alonso and Eusebio Bernabéu

Department of Optics, Universidad Complutense de Madrid,
Faculty of Physics, Ciudad Universitaria s/n, 28040 Madrid, Spain
luqueras@telefonica.net

Abstract: The pseudo-imaging process in a system consisting of two periodic gratings and illuminated by an incoherent polychromatic and finite extension source placed at a finite distance from the gratings is studied. An analytical expression of the irradiance distribution on a plane, also located at a finite distance from the gratings, has been obtained from previous results on monochromatic illumination. In the analysis presented, different imaging regimes are found and related to the parameters which characterize the double grating system. The pseudo-imaging phenomenon strongly depends on both the spatial and temporal coherence of the incident illuminating field. Certain pseudo-images are observed with polychromatic and incoherent incident light under some restrictions. On the other hand, pseudo-image process analogous to Talbot effect appears only by monochromatic and plane illuminating wavefront.

©2004 Optical Society of America

OCIS codes: (050.1940) Diffraction; (050.2770) Gratings.

References and Links

1. F. Talbot, "Facts relating to optical science. No. IV," Philos. Mag. **9**, 401-407 (1836).
2. J. M. Cowley and A. F. Moodie, Proc. R. Soc. London Ser. B **70,** 486 (1957).
3. E. Keren, O. Kafri, "Diffraction effects in moire deflectometry," J. Opt. Soc. Am. A **2**, 111-120 (1985).
4. S. Teng, L. Liu, J. Zu, Z. Luan, and De'an Liu, "Uniform theory of the Talbot effect with partially coherent light illumination," J. Opt. Soc. Am. A **20,** 1747-1754 (2003).
5. E. Lau. "Beugungserscheinungen an Doppelrastern," Ann. Phys. (Leipzig) **6**, 417-423 (1985).
6. J. Jahns and A.W. Lohmann, "The Lau effect (a diffraction experiment with incoherent illumination," Opt. Commun. **28,** 263-267 (1979).
7. F. Gori, "Lau effect and coherence theory," Opt. Commun. **31**, 4-8 (1979).
8. R. Sudol and B.J. Thompson, "An explanation of the Lau effect based on coherence theory," Opt. Commun. **31,** 105-110 (1979).
9. K.H. Brenner, A.W. Lohmann and Ojeda-Castaneda, "Lau effect: OTF theory," Opt. Commun. **46,** 14-17 (1983).
10. L. Liu, X. Liu and L. Ye, "Joint Talbot effect and logic operated moire patterns," J. Opt. Soc. Am. A **7,** 970-976 (1990).
11. L. Liu, "Interferometry based on the partially coherent effect lying between the Talbot and Lau effects," J. Mod. Opt. **35,** 1605-1618 (1988).
12. L. Liu, "Partially coherent diffraction effect between Lau and Talbot Effects," J. Opt. Soc. Am. A **5,** 1709-1716 (1988).
13. K. V. Avudainayagam and S. Chitralekha, "Lau effect and beam collimation," J. Mod. Opt. **44,** 175-178 (1997).
14. M. Tebaldi, L. Angel Toro and N. Bolognini, "Interferometry based on Lau effect with a grating registered in a photorefractive crystal," Opt. Las. Tech. **31,** 127-134 (1999).
15. D. Crespo, J. Alonso, T. Morlanes and E. Bernabéu, "Optical encoder based on the Lau effect," Opt. Eng. **39**, 817-824 (2000).
16. J. Pomarico, R. Torroba, "Colour image operations based on white light diffraction experiments (Lau effect)", Eur. J. Phys. **14**, 114-120 (1993).
17. L. Liu, "Talbot and Lau effects on incident beams of arbitrary wavefront, and their use," Appl. Opt. **28**, 4668-4677 (1989).
18. K. Patorski, "The self-imaging phenomenon and its applications," in *Progress in Optics*, E. Wolf, ed. (North Holland, Amsterdam 1989) vol. 27, pp. 3-108.
19. K. Patorski, "Incoherent superposition of multiple self-imaging Lau effect and moire fringes explanation," Opt. Acta **30,** 745-758 (1983).

#4362 - $15.00 US Received 13 May 2004; revised 22 May 2004; accepted 25 May 2004
(C) 2004 OSA

20. G. J. Swanson and E. N. Leith, "Lau effect and grating imaging," J. Opt. Soc. Am. **72**, 552-555 (1982).
21. G. J. Swanson and E. N. Leith, "Analisys of the Lau effect and generalized grating imaging," J. Opt. Soc. Am. A **2**, 789-793 (1985).
22. S.C. Som and A. Satpathi, "The generalized Lau effect," J. Mod. Opt. **37,** 1215-1226 (1990).
23. L. Liu, "Ambiguity function and general Talbot-Lau effects," Acta Opt. Sin. **7,** 501-510 (1987).
24. J. Tu and L. Zhan, "Two-dimensional theory of the Lau-Talbot-Moiré effect under partially coherent illumination," Opt. Commun. **82,** 229-235 (1991).
25. J. Tu and L. Zhan, "Analysis of general double periodic structure diffraction phenomena based on the ambiguity function," J. Opt. soc. Am. A **9,** 983-995 (1992).
26. A. Olszak and L. Wronkowski, "Analysis of Fresnel field of a double diffraction system in the case of two amplitude diffraction gratings under partially coherent illumination," Opt. Eng. **36**, 2149-2157 (1997).
27. D. Crespo, J. Alonso and E. Bernabéu, "Generalized imaging using an extended monochromatic light source," J. Opt. Soc. Am. A **17**, 1231-1240 (2000).
28. D. Crespo, J. Alonso and E. Bernabéu, "Experimental measurements of generalized grating images," Appl. Opt. OT **41,** 1223-1228 (2002).

1. Introduction

It is well known that light fields with lateral periodicity also present longitudinal periodicity. There are a number of phenomena in which this general property is revealed: self-imaging or Talbot effect, joint Talbot effect, Lau effect, incoherent grating-lens imaging, misfocused diffraction convolution and generalized Lau effect or pseudo-imaging [1-9]. Many applications are based on these effects: e.g., moiré deflectometry and metrology, Talbot interferometry and a number of spectroscopic techniques based on Talbot and Lau effects are known and widely used [10-18].

Most of the mentioned phenomena involve the transmission of coherent or partially coherent light through linear gratings. When the irradiance distribution across a transversal plane is constant in the region of interest, the transmission through each grating forces the field to be laterally periodic, with a period identical to that of the grating. The primary consequence of this condition is the formation of self-images which is called the Talbot effect. Within the Fresnel approximation, assuming the light to be monochromatic and coherent, and the grating to be infinite, self-imaging extends to all the space behind the grating. Partial coherence, polychromaticity or finite extension of the gratings causes the self-images to be partially or totally degraded. Non uniform irradiance profiles have also been studied by Liu [17]. A thorough and comprehensive review of the self-imaging phenomenon is due to Patorski [18].

The Lau effect involves the use of two identical gratings and an incoherent source. A fringe pattern with period and profile different to those of the gratings (usually considered as a pseudo-image of the first grating) is observed at infinity, that is, at the focal plane of a lens located behind the second grating [5-9]. When the periods of the gratings are different, fringe patterns are formed, without the need for a lens, at finite grating conjugates. More fringe patterns are also formed at positions which satisfy a higher order finite conjugate relation (involving two integer indexes) even for gratings with equal periods. This effect is called pseudo-imaging or generalized Lau effect.

Pseudo-imaging has been extensively analyzed by a number of authors [19-28]. All the models are based on the Fresnel (paraxial) approximation for the propagation of a monochromatic field. The first analysis of pseudo-imaging is due to Patorsky [19]. He used a model in which the first grating is considered a collection of incoherent line sources. Pseudo-images then appear as a result of the superposition of multiple incoherent self-images of the second grating. The indexing of many different pseudo-images, their position and their relationship with the periods of the gratings and the distance between them, was addressed by Swanson and Leith [20,21]. They used a source model in which the contributions of plane waves with uniform distribution of the transversal component of the wave vector add incoherently. Som and Satpathi [22], use a model based on the point spread function for a periodic object, and then they reconstruct self-imaging, for the totally coherent case with a single grating, and Lau effect and pseudo-imaging with two gratings, for the totally incoherent case.

#4362 - $15.00 US Received 13 May 2004; revised 22 May 2004; accepted 25 May 2004
(C) 2004 OSA

Partial coherence at the first grating has been taken into account by means of the ambiguity function [24,25], the complex degree of mutual coherence [26], or by calculating and incoherently adding the contribution from each point of a finite extension source [27,28]. Also, Tu and Zhan [25], and Olszak and Wronkowski [26], consider the lack of parallelism between the gratings. Regardless of whether the electromagnetic field or a phase-space distribution function is used, the Fresnel approximation is applied for light propagation through the gratings from the source to the observation plane. The resulting formula for the irradiance in a double grating system is rather complex and involves a sum extended to four indexes. As a consequence, the understanding of the effect of the different parameters on the pseudo-imaging phenomenon is a difficult task. This problem was addressed in the work by Crespo [27,28], in which some approximations lead to a simplified version of the general expression for the irradiance at the observation plane. This work also contains an analysis of the depth of focus of the pseudo-images, showing that many of the indexed pseudo-images predicted by the models based on totally incoherent illumination really merge into a larger depth of focus pseudo-image.

In the present work two objectives are pursued: first, the understanding of the influence of a finite bandwidth in the frequency spectrum of the source. Talbot and Lau effects have been investigated under polychromatic sources [3,16], but to our knowledge, there are no similar studies for pseudo-imaging. In this work a generalization of the formula derived in references [25] to [27], which include polychromatic sources, is presented. Second, extensive computing of the obtained expression is performed to provide the irradiance distribution, and from it the contrast of the pseudo-images as a function of the distance between gratings and the observation position. This computation is carried out for several values of the size, position and spectral bandwidth of the polychromatic source. The result is a general survey of the pseudo-imaging phenomenon in which transitions from coherent to partially coherent to incoherent illumination, and from monochromatic to polychromatic fields, are made clear on a graphical basis.

2. Description of the two-grating optical system

The optical system studied in this work is shown in Fig. 1. It consists of a finite extension and polychromatic light source and two gratings, G_1 and G_2, with arbitrary periods. We will consider the source to be made up of a continuum of point sources which are mutually incoherent. We want to determine the light distribution on the observation plane as well as to study the influence of each one of the parameters involved in the pseudo-imaging process; in particular, the dependences on the source characteristics and the geometrical parameters describing the system.

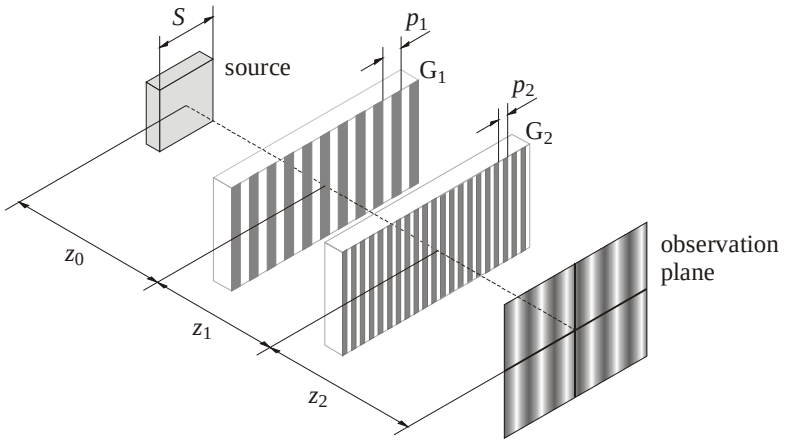

Fig. 1. Optical system studied.

#4362 - $15.00 US Received 13 May 2004; revised 22 May 2004; accepted 25 May 2004
(C) 2004 OSA

The grating planes and the observation plane are all parallel and perpendicular to the propagation direction, the *z*-axis. We assume that the lines of both gratings are also parallel, and the *x*-axis is set perpendicular to these lines. The distance between the source and the first grating G_1 is named z_0. The distance between both gratings, G_1 and G_2, is z_1, and the relative position between them along the *x*-axis is Δx. The observation plane is placed at a distance z_2 from the grating G_2. To shorten the formulas, we will make the definitions $z_{01} \equiv z_0 + z_1$, $z_{12} \equiv z_1 + z_2$ and $z_t = z_0 + z_1 + z_2$. The size of the source along the *x*-direction is *S*.

3. Irradiance at the observation plane

Within the thin-grating approximation, both gratings, G_1 and G_2, are characterized by their complex transmittances. Let $t_1(x)$ and $t_2(x)$ be such transmittances. No assumption is made on the amplitude or phase profile of these gratings except that they are periodic, with periods p_1 and p_2 respectively. The Fourier expansion for such transmittances can be expressed as

$$t_1(x) = \sum_n a_n \exp\left(i\,2\pi n x / p_1\right) \text{ and } t_2(x) = \sum_n b_n \exp\left(i\,2\pi n x / p_2\right) \tag{1}$$

According to the model by Crespo, Alonso and Bernabéu [27], under monochromatic illumination of wavelength λ and within the Fresnel approximation, the irradiance at the observation plane can be written as

$$I_\lambda(x) = \sum_{nlmk} A_{nlmk} \exp\left(iB_{nlmk}\lambda\right), \tag{2}$$

where the magnitudes A_{nlmk} and B_{nlmk} are given by

$$\begin{aligned} A_{nlmk} = a_n a_l^* b_m b_k^* \exp\left\{ i \frac{2\pi x}{p_1 z_t}\left[z_0(n-l) + R z_{01}(m-k)\right]\right\} \\ \times \operatorname{sinc}\left\{ \frac{2\pi S}{p_1 z_t}\left[z_{12}(n-l) + R z_2 (m-k)\right]\right\} \end{aligned} \tag{3a}$$

and

$$B_{nlmk} = \frac{\pi}{p_1^2 z_t}\left[z_0 z_{12}\left(n^2 - l^2\right) + R^2 z_2 z_{01}\left(m^2 - k^2\right) + 2R z_0 z_2 (nm - lk)\right]. \tag{3b}$$

R is defined as the quotient between the two periods, $R \equiv p_1/p_2$.

In the case of a polychromatic source with normalized spectrum $g(\lambda)$ the total irradiance is given by

$$\begin{aligned} I(x) &= \int_{-\infty}^{+\infty} g(\lambda) I_\lambda(x) \mathrm{d}\lambda \\ &= \sum_{nlmk}\left[\int_{-\infty}^{+\infty} g(\lambda) A_{nlmk}(\lambda) \exp\left(iB_{nlmk}\lambda\right)\mathrm{d}\lambda\right]. \end{aligned} \tag{4}$$

For amplitude gratings, the coefficients A_{nlmk} does not depend on the wavelength, therefore

$$I(x) = \sum_{nlmk}\left[A_{nlmk} G\left(-B_{nlmk}\right)\right], \tag{5}$$

where G is the Fourier transform of $g(\lambda)$. We will assume that the spectrum of the light source is gaussian, centered at λ_0 and of width $\Delta\lambda$. The normalized spectrum is therefore given by

#4362 - $15.00 US
Received 13 May 2004; revised 22 May 2004; accepted 25 May 2004
(C) 2004 OSA

$$g(\lambda) = \frac{1}{\sqrt{2\pi(\Delta\lambda)^2}} \exp\left[-\frac{(\lambda - \lambda_0)^2}{2(\Delta\lambda)^2} \right]. \tag{6}$$

Computation of the total irradiance is then straightforward, with the result

$$I(x) = \sum_{nlmk} A_{nlmk} \exp\left[B_{nlmk} \left(i\lambda_0 - \frac{B_{nlmk}(\Delta\lambda)^2}{2} \right) \right]. \tag{7}$$

Note that Eq. (3) is recovered if $\Delta\lambda \to 0$ i.e., when the illuminating light is monochromatic.

Equation (7) allows us to obtain the irradiance profile at any position of the observation plane. In general, it will be a periodic function of the *x*-axis. Finally, we define the contrast of the pseudo-image in the observation plane as usual,

$$C = \frac{\max[I(x)] - \min[I(x)]}{\max[I(x)] + \min[I(x)]}. \tag{8}$$

4. Numerical analysis: Ronchi gratings

The results of the most accurate models currently available to describe the pseudo-imaging phenomenon are summarized in Eq. (2) and (7). In the references [22] to [27] we find equivalent or identical results than Eq. (2) obtained with different approaches. The present work generalizes such equation to polychromatic light.

Equation (7) is rather complex, and it is difficult to obtain conclusions directly from such an expression. For that reason, we have made an extensive numerical analysis of the same. There are many parameters entering Eq. (7), that can be grouped in three different sets: geometric parameters, which are the distance between gratings and the distance to the observation plane; parameters of the illuminating light, which are the position and size of the source (spatial coherence), the spectral width (temporal coherence) and the central wavelength. The last set of parameters describes the gratings: periods, relative displacement along the *x*-direction, and phase and transmitance profiles, these last being encoded in the coefficients of the Fourier expansion. In order to reduce degrees of freedom, we restrict this work to the important case of Ronchi gratings. We have written an optimized program which computes the irradiance $I(x)$ along the *x*-direction on the observation plane. Distributed in the aforementioned groups, the input parameters for this program are $\{z_1, z_2\}$, $\{z_0, S, \lambda_0, \Delta\lambda\}$ and $\{p_1, p_2, \Delta x\}$. The analysis generates a huge amount of data and from them, we have concluded that the pseudo-imaging phenomenon scales smoothly with the grating periods and the central wavelength, while it shows strong dependence on the light coherence (both spatial and temporal), as well as on the distances z_1 and z_2. For this reason, and to help interpret this information, we compute and represent the contrast of the irradiance distribution on the observation plane for a continuous of values of the geometric parameters, (z_1, z_2), and generate color plots of the function $C(z_1, z_2)$. Different contour plots have been generated for different values of the spatial and temporal coherence of the incident light field, within a complete scan of all the available lighting conditions. Each point in any of the following colour plots stands for a completely defined configuration of the double grating system shown in Fig. 1. The value encoded for this point according to the colormap shown in Fig. 2 equals the contrast of the pseudo-image obtained at the observation plane for the specific configuration. All the colour plots in this work share the same colormap.

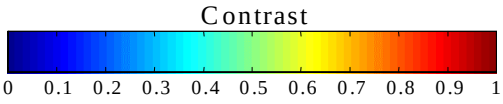

Fig. 2. Colormap used thorough this work for all the color plots of $C(Z_1, Z_2)$.

#4362 - $15.00 US
Received 13 May 2004; revised 22 May 2004; accepted 25 May 2004
(C) 2004 OSA

5. Coherence of the illuminating field: limiting cases

We will first present a set of eight limiting cases for the three parameters controlling the coherence of the incident light, $\{z_0, S, \Delta\lambda\}$. We will next explore the transition between these limiting cases. The limits for each parameter are $z_0 \in [250\ \mu m, 10^3\ m]$, $S \in [0, 10^3\ m]$, $\Delta\lambda \in [0, 400\ nm]$. The limit of 10^3 m for both source distance and source size stands for infinity in our simulation, as larger values did not have any observable effect on the contrast. Also, when the source is punctual, the distance $z_0 = 0$ is not valid because it overrides the first grating, transforming the problem in a single grating Talbot effect with spherical wave. For infinitely large sources, $z_0 = 0$ and $z_0 = 250\ \mu m$ are indistinguishable. Finally, we have chosen a spectral width similar to that of the visible spectrum to characterize a field with a coherence length similar to the wavelength, that is, totally incoherent in the temporal sense. For these limiting cases we have selected equal Ronchi gratings with period $p_1 = p_2 = 10\ \mu m$. Central wavelength has been set to 400 nm. In each figure from Fig. 3 to 6 we present two plots for the two limiting cases of the spectral width. We have also normalized the distances z_1 and z_2 to the Talbot distance for the first grating, p_1^2/λ, obtaining the dimensionless parameters $Z_i = z_i\lambda/p_1^2$, $i = 1, 2$.

From the contrast data shown in Fig. 3 to Fig. 6, the pseudo-imaging phenomenon can be classified in three different regimes. When the illuminating field is a monochromatic spherical wave, (Fig. 3(a)), pseudo-images with high contrast appear for almost all positions of the gratings and the observation plane. With a punctual and polychromatic source (Fig. 3(b)), pseudo-images also appear for all values of Z_1 and small values of Z_2. Note that in this case, when the two gratings are in contact (which is equivalent to a single grating), the contrast decreases rapidly as Z_2 increases. However, if the second grating is located at the first Talbot plane of the first one, the contrast of the fringes formed behind it decreases more slowly; even a local maxima of contrast can be observed at the first Talbot plane of the second grating. In any two cases, pseudo-images are continuously and broadly distributed in the plane (Z_1, Z_2).

The second regime is produced with a plane and monochromatic wave (Fig. 4(a)). With this illumination, the Talbot effect commands the pseudo-image formation as the contrast reaches a maximum at the Talbot planes of the second grating. In the case of no relative displacement between both gratings, when G_2 is located at any even order Talbot plane of G_1, all the flux coming from the first grating passes through the second one. At any odd order Talbot plane, there is a shift of the self-image of $p_1/2$, so no light goes through G_2 and contrast computation becomes inaccurate. At any other position of G_2, some light coming from G_1 is stopped by G_2, but high contrast self-images are formed at the Talbot planes of the second grating. For that reason, maximum contrast is obtained along any horizontal line located at integer values of Z_2 in the plot of Fig. 4(a), except for the odd integer values of Z_1.

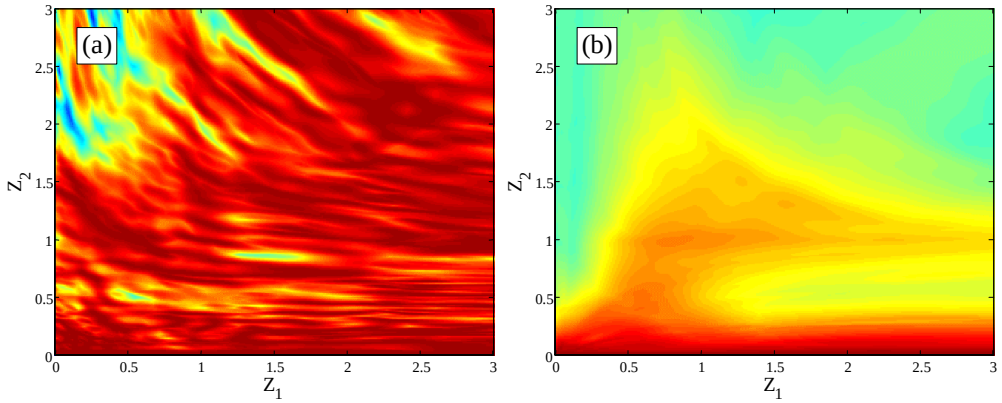

Fig. 3. Pseudo-image contrast for $z_0 = 250\ \mu m$ and $S = 0$. (a) $\Delta\lambda = 0$; (b) $\Delta\lambda = 400$ nm.

#4362 - $15.00 US
Received 13 May 2004; revised 22 May 2004; accepted 25 May 2004
(C) 2004 OSA

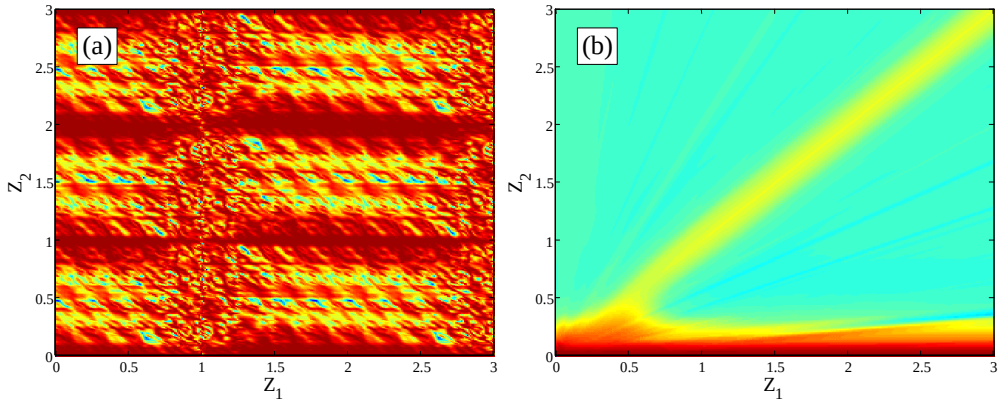

Fig. 4. Pseudo-image contrast for $z_0 \to \infty$, $S = 0$ and $\Delta x = 0$. (a) $\Delta\lambda = 0$; (b) $\Delta\lambda = 400$ nm.

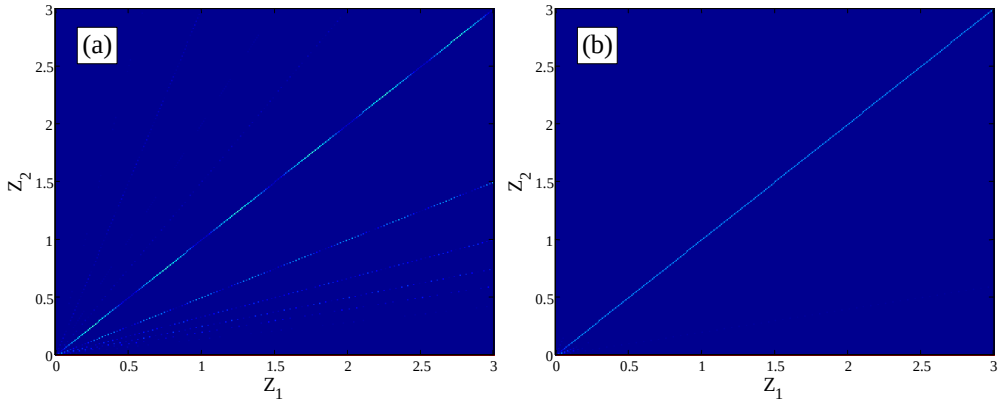

Fig. 5. Pseudo-image contrast for $z_0 = 250$ μm and $S \to \infty$. (a) $\Delta\lambda = 0$; (b) $\Delta\lambda = 400$ nm.

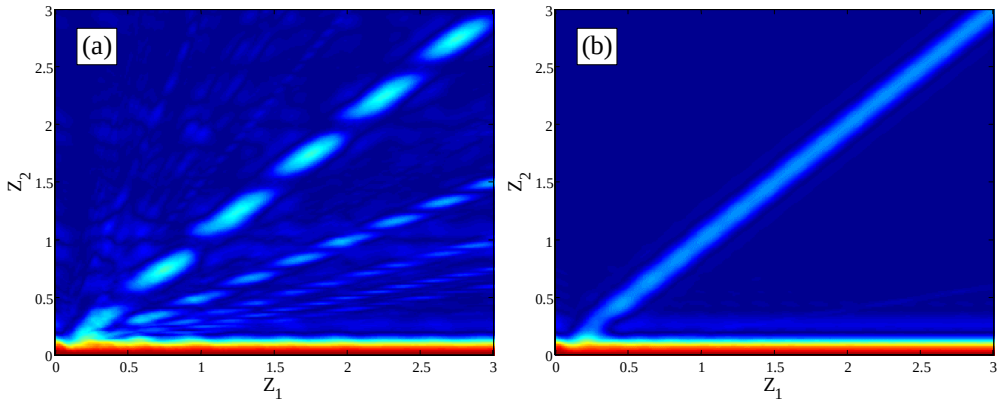

Fig. 6. Pseudo-image contrast for $z_0 \to \infty$, $S \to \infty$ and $S/z_0 = 0.1$. (a) $\Delta\lambda = 0$; (b) $\Delta\lambda = 400$ nm.

In the third regime, isolated pseudo-images are obtained for values of Z_1 and Z_2 satisfying the relation $Z_2 = k\,Z_1$, k being a constant. This behavior can be observed in Fig. 5(a) and 5(b) (large source at a close distance) and Fig. 6(a) and 6(b) (large source infinitely far away), both characterized for the spatial incoherence of the illuminating beam. Pseudo-images whose positions satisfy the relation $Z_2 = k\,Z_1$ were first predicted and indexed by Swanson and Leith

#4362 - $15.00 US
Received 13 May 2004; revised 22 May 2004; accepted 25 May 2004
(C) 2004 OSA

[21,22]. They assumed an illuminating beam composed of independent (incoherent) plane waves with uniformly distributed incidence angle. This theoretical source model has been associated by some authors to an infinitely large source located at infinite distance from G_1 [7-9]. As we demonstrate below, this interpretation must be slightly re-formulated, as the pseudo-imaging phenomenon will belong to any of the three regimes depending on the limiting value of the quotient z_0/S, when both z_0 and S tend to infinity. According to the van Cittert-Zernike theorem, this limit determines the spatial coherence of the incident field at G_1.

The result formulated in Eq. (7) has allowed us to extend previous results to polychromatic light. Three main conclusions can be readily obtained from the presented limiting cases:

1. Some pseudo-images which appear with monochromatic spatially incoherent light, disappear when polychromaticity is introduced. When the periods of the two gratings are equal, only the pseudo-image satisfying $Z_2 = Z_1$ survives.
2. The surviving pseudo-image becomes "stable", i.e. the contrast value of this pseudo-image along the line $Z_2 = Z_1$ does not depend on Z_1. With monochromatic light, a periodic modulation of the contrast is observed for pseudo-images within the third regime (Fig. 5(a) and 6(a)): at regular intervals of Z_1, whose length depends on the slope of the pseudo-image, the contrast decreases to negligible values. This fluctuation of the pseudo-imaging phenomenon disappears for the pseudo-image which remains when polychromatic light is used.
3. Under collimated light, polychromaticity changes the pseudo-imaging from the second regime (Fig. 4(a)) to the third regime (Fig. 4(b)). In this case a stable pseudo-image with contrast $C \approx 0.65$ appears for $Z_1 = Z_2$. This pseudo-image has a much larger depth of focus than those obtained with large sources (non collimated illumination).

6. Pseudo-imaging with a finite extension source

We study in this section the pseudo-imaging with finite extension sources in a greater detail. As analyzed in the work by Crespo and co-workers, the sinc function appearing in the coefficients A_{nmlk} is responsible for the pseudo-imaging within the third regime. This function reaches its maxima when the argument becomes zero, that is, when the pseudo-imaging condition, $n(z_1 + z_2) - Rmz_2 = 0$ is met, n and m being two integers small enough to satisfy

$$\frac{S}{z_T} > n\frac{p_2}{2z_2} \quad \text{and} \quad \frac{S}{z_T} > m\frac{p_1}{2(z_1 + z_2)}. \tag{9}$$

These inequalities can be interpreted as follows: for a pseudo-image with indexes (n, m) to have significant contrast, the angle subtended by the source from the observation plane must be larger than n times the angle subtended by one slit of the second grating and larger than m times the angle subtended by one slit of the first grating, both from the observation plane. The pair (n, m) will be the order of the pseudo-image. The pseudo-image condition can be rewritten as

$$z_2 = \left(\frac{m}{n}\frac{p_1}{p_2} - 1\right)^{-1} z_1, \tag{10}$$

so the slope of the pseudo-image depends on the quotient m/n. Pseudo-images of order (qn, qm), with q integer, are superimposed.

In Fig. 7 we have indexed pseudo-images corresponding to a finite extension monochromatic source at finite distance. The size of the source is 300 μm, that of a typical LED. The pseudo-image pattern is very similar to that of Fig. 5(a), though the source size is completely different. This is because inequalities in Eq. (9) are fully satisfied for lowest order pseudo-images even for a 300 μm source (at close distance). For larger sources we could expect higher order pseudo-images satisfying Eq. (9), but the numerical results demonstrate that the contrast becomes negligible for orders higher than those listed in Fig. 7.

Another result is that the depth of focus of the pseudo-images (range of Z_2 for which contrast remains large) increases with Z_1. We also observe that depth of focus decreases as the

#4362 - $15.00 US Received 13 May 2004; revised 22 May 2004; accepted 25 May 2004
(C) 2004 OSA

source becomes larger. In the limit case, when the extension of the source is infinite, depth of focus goes to zero, as it was predicted by Crespo et al., and confirmed in Fig. 5(a).

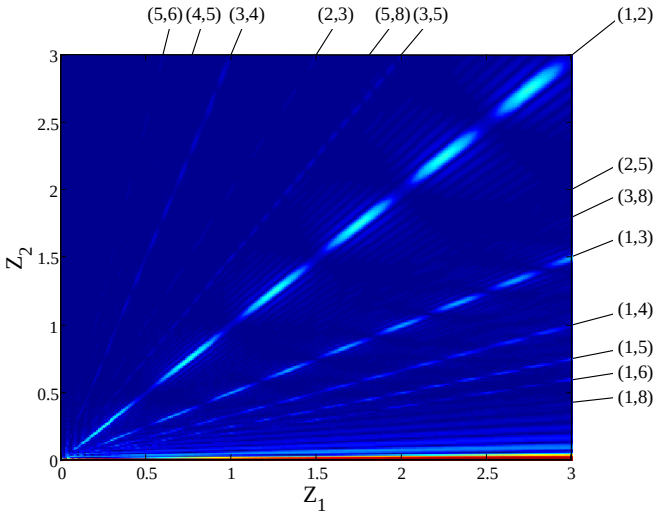

Fig. 7. Pseudo-image indexing. z_0 = 250 μm, S = 300μm, Δλ = 0 and λ = 400 nm.

From data obtained for pseudo-images within the third regime with monochromatic sources, we have empirically quantified the period of the contrast fluctuations along Z_1 for each pseudo-image. We will name $(Z_1)_{\min}^{nm}$ and $(Z_1)_{\max}^{nm}$ to the values of Z_1 for which the contrast reaches minima and maxima, respectively, in the (n, m) pseudo-image. When n is odd and m even, we find

$$\begin{aligned} \left(Z_1\right)_{nm}^{\min} &= \frac{1}{Rnm}(k+1), \\ \left(Z_1\right)_{nm}^{\max} &= \frac{1}{2Rnm}(2k+1), \quad k = 0,1,2,\ldots \end{aligned} \tag{11a}$$

whereas for m odd

$$\begin{aligned} \left(Z_1\right)_{nm}^{\min} &= \frac{1}{2Rnm}(2k+1), \\ \left(Z_1\right)_{nm}^{\max} &= \frac{1}{Rnm}k, \quad k = 0,1,2,\ldots \end{aligned} \tag{11b}$$

All other cases in which n and m are even can be reduced to equivalent cases described above. By means of some approximations applied on Eq. (2), Crespo et al. obtained an analytical expression for the position of the maxima for pseudo-images with m odd, in full agreement with Eq. (11b). To our knowledge, the case for n odd and m even was not treated before.

When finite spectral width is introduced, the effect is the same as shown in Fig. 5(b) and Fig. 6(b). The periodic fluctuation of the contrast gets damped, and decreases to zero for all pseudo-images except for the (1, 2), for which contrast stabilizes at a value of 0.27. Depth of focus does not depend on the spectral width for this pseudo-image. Also it has not been observed any displacement of the points of maximum and minimum contrast in the pattern (defined by Eq. 11) when the spectral bandwidth of the light is increased. The effect is better shown in Fig. 8, in which contrast has been computed along the straight line given by Eq. (10) for pseudo-images (1, 2) and (1, 3). With grating periods of 10 μm, a spectral width of 50 nm is enough to make the contrast of the (1, 2) pseudo-image stable for $Z_1 > 2$. Another

#4362 - $15.00 US
Received 13 May 2004; revised 22 May 2004; accepted 25 May 2004
(C) 2004 OSA

simulations not shown to avoid cluttering up the paper with figures, demonstrate that the larger the periods of the gratings, the larger the spectral width necessary to stabilize the contrast at some Z_1. Similarly, at a fixed spectral width, larger periods require larger values of Z_1 to get the contrast stable.

When the periods are not equal, a different number of pseudo-images are supported. According to Eq. (10), the condition $mp_1/np_2 > 1$ must be met for the pseudo-image to be real, that is, for the pseudo-image may form with a positive value of z_2.

The larger the value of p_1 with respect to p_2, the larger the number of pseudo-images supported. In Fig. 9(a) we present a computation of contrast with the same parameters previously used in Fig. 7, except for p_1 which has been set to 30 μm. The slope of the pseudo-image (1, 2) is now 1/5. With this setting, the high contrast pseudo-image (1, 1) is now real, with a slope 1/2. The pseudo-images (1, *m*), (2, 5) and (3, 8), indexed in the Fig. 7, are now "compressed" with small slopes under the pseudo-image (1, 2).

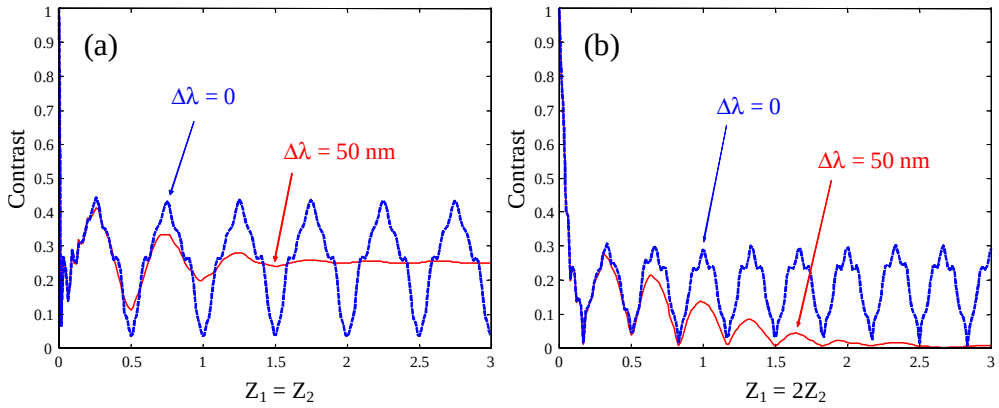

Fig. 8. (a) Contrast of the pseudo-image (1, 2) with monochromatic (blue) and polychromatic (red) illumination. Parameters: $p_1 = p_2 = 10$ μm, $z_0 = 250$ μm, $S = 300$ μm, $\lambda_0 = 400$ nm. The spectral width of the polychromatic source is 50 nm. (b) The same for the pseudo-image (1, 3).

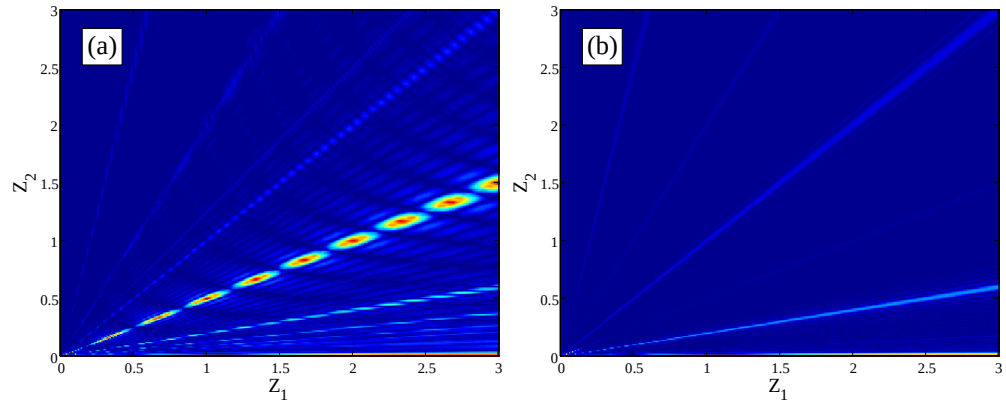

Fig. 9. Pseudo-images obtained with periods $p_1 = 30$ μm and $p_2 = 10$ μm. (a): Monochromatic light, parameters $z_0 = 250$ μm, $S = 300$ μm, $\lambda_0 = 400$ nm. (b): Same parameters than (a) except for $\Delta\lambda = 400$ nm.

#4362 - $15.00 US
Received 13 May 2004; revised 22 May 2004; accepted 25 May 2004
(C) 2004 OSA

We present in Fig. 9(b) the effect of a finite spectral width. As in the previous cases, many pseudo-images disappear, but it is also observed a stabilization of the contrast in more orders than the (1, 2). In particular, orders of the type (n, 2), with n = 1,...,5, are appreciated in Fig. 9. Simulations carried out with larger values of p_1 and with a larger number of Fourier coefficients used in Eq. (7) to increase accuracy, demonstrate that stabilization of orders (n, 2) happens for even higher values of n.

7. Intermediate cases

In order to complete the analysis of pseudo-imaging with arbitrary coherence sources, we present the main results obtained from extensive computation of Eq. (7) with coherence parameters ranging between the limiting cases previously shown. As the monochromatic and "white light" cases were included in the limiting cases, we will select a quasi-monochromatic source with a spectral width $\Delta\lambda$ = 60 nm, typical of many LEDs. In Fig. 10 we analyze the effect of the source size, with parameters $p_1 = p_2$ = 10 μm, z_0 = 250 μm, λ_0 = 400 nm, $\Delta\lambda$ = 60 nm. With S = 0, pseudo-imaging belongs to the first regime, as in the case shown in Fig. 3(a). The first frame of Fig. 10 is then an intermediate case between those in Fig. 3(a) and Fig. 3(b). With just a source size of 18 μm (Fig. 10(c)), the third pseudo-imaging regime is recognizable. S = 10 μm is in the transition between both regimes (Fig. 10(b)). From source sizes of 100 μm on, pseudo-images of the type $Z_2 = kZ_1$ are clearly visible, although, because of the spectral width of 60 nm with which the contrast has been computed, only the order (1, 2) is clearly visible in Fig. 10(d).

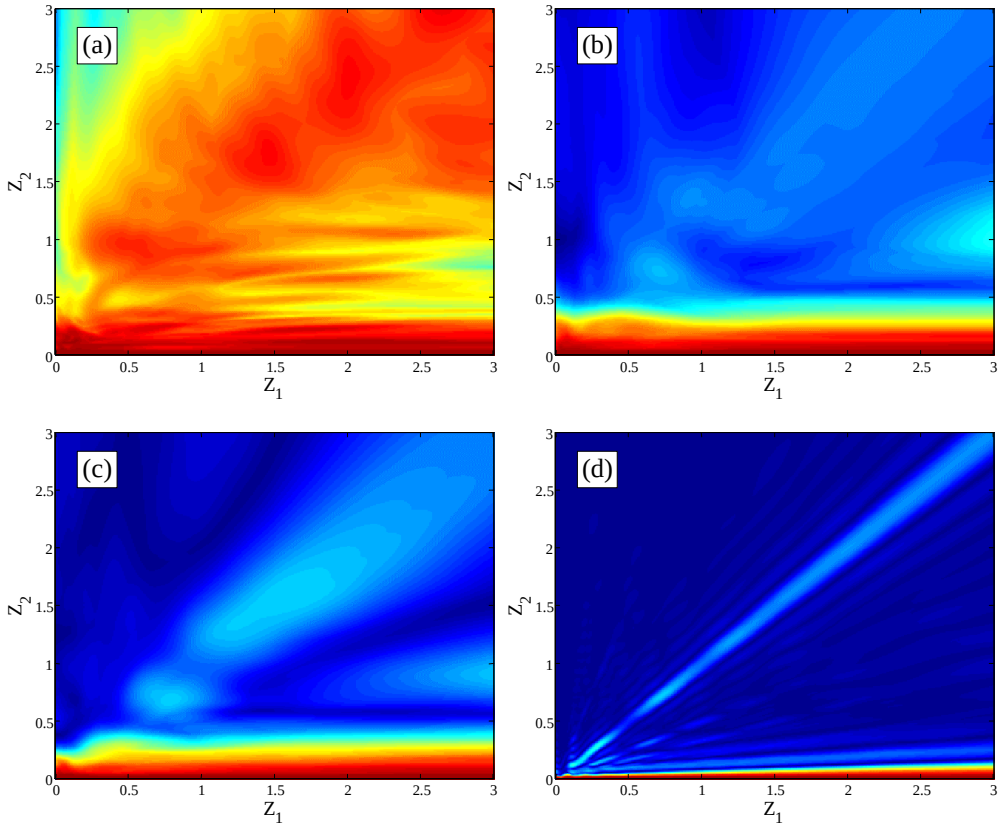

Fig. 10. Effect of the source size. $p_1 = p_2$ = 10 μm, z_0 = 250 μm, λ_0 = 400 nm and $\Delta\lambda$ = 60 nm. (a): S = 0; (b): S = 10 μm; (c): S = 18 μm; (d): S = 116 μm.

#4362 - $15.00 US
Received 13 May 2004; revised 22 May 2004; accepted 25 May 2004
(C) 2004 OSA

The effect of the source position is analyzed in Fig. 11. The parameters are the same than in previous figure, but source size is now fixed to 300 μm, and z_0 takes the values 1, 10, 20 and 10^4 mm in the four plots. In the first plot, with the source at 1 mm from the first grating, pseudo-imaging belongs to the third regime. For this LED-type source, the transition to the second regime (collimated light) begins at z_0 = 10 mm, for which we begin to appreciate the first Talbot plane of the second grating, at Z_2 = 1. The last plot clearly corresponds with the second regime. From z_0 = 10 m on, no changes are appreciated in the contrast map, and pseudo-imaging reaches a stationary behaviour within regime 2.

To finish this analysis, we comment some results relative to the dependence of pseudo-imaging on the quotient S/z_0. As we said before, the spatial coherence of the incident field depends on the source size and on the source position. We have found that for large values of z_0, the contrast only depends on the quotient S/z_0, although for small values of z_0 both parameters become uncoupled. When the quotient S/z_0 tends to infinity as S and z_0 increases, pseudo-imaging stays in the third regime, as shown in Fig. 6(a) and 6(b). When S/z_0 tends to zero as S and z_0 increases, pseudo-imaging stays in the second regime (that of collimated light), as shown in Fig. 4(a) and 4(b). As an intermediate example, the second frame of Fig. 11 was computed with a quotient S/z_0 = 0.03. We have performed computations of the contrast with the same parameters, keeping the quotient S/z_0 fixed and ranging S from 10 μm to 10^3 m. From a source size of 100 μm (located at 3.33 mm) on, the contrast map does not change.

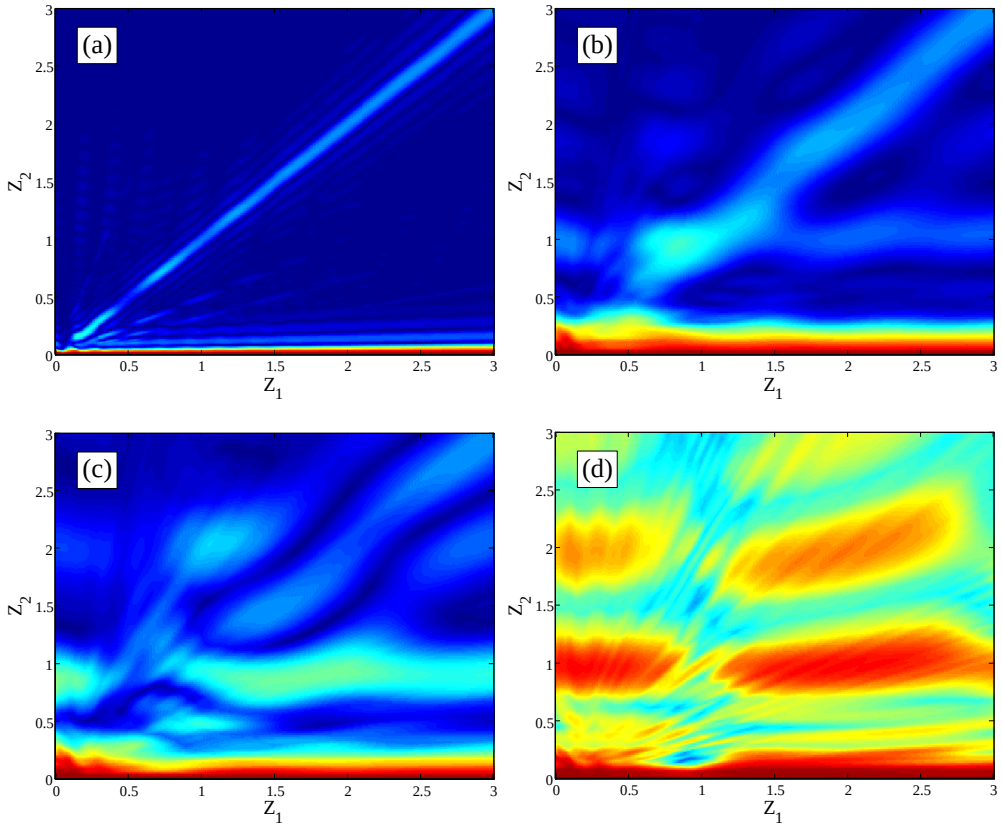

Fig. 11. Effect of the source location. $p_1 = p_2$ = 10 μm, S = 300 μm, λ_0 = 400 nm and $\Delta\lambda$ = 60 nm. (a): z_0 = 1 mm; (b): z_0 = 10 mm; (c): z_0 = 20 mm; (d): $z_0 = 10^4$ mm.

#4362 - $15.00 US
Received 13 May 2004; revised 22 May 2004; accepted 25 May 2004
(C) 2004 OSA

8. Conclusions

A general analytical expression has been obtained for computing the irradiance distribution in a typical double grating system, illuminated by a polychromatic and finite extension source. The expression is valid for arbitrary amplitude gratings, for which the integration over wavelengths can be carried out. Extensive numerical computations have been performed in order to uncover the nature of the pseudo-imaging process, mainly in relation to the coherence of the incident light. Size, location and spectral bandwidth of the source are the parameters employed to vary the spatial and temporal coherence of the incident light.

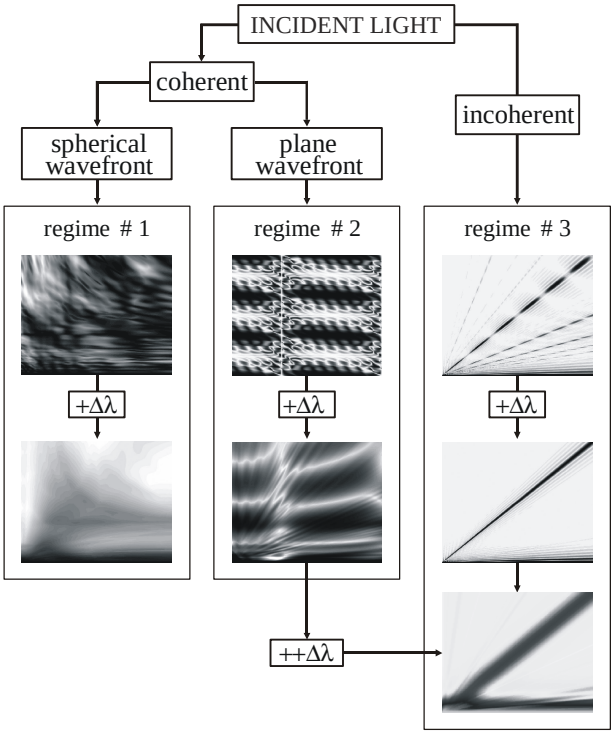

Fig. 12. Graphical summary of the distribution of pseudo-imaging into different regimes, and its relation with the coherence of the incident field.

We have found that pseudo-imaging may be classified into three different regimes, as summarized in Fig. 12. The first one occurs under coherent and spherical waves, and pseudo-images are located without restrictions on the distance between gratings or the position of the observation plane. The second regime is produced under monochromatic or pseudo-monochromatic plane waves. Within this regime, pseudo-imaging can be explained as a consequence of the Talbot effect. Finally, in the third regime, localized pseudo-images at $Z_2 = kZ_1$ appear. In this case, incident light must be incoherent. Polychromaticity has different effects in each regime. In the two first, the contrast of the pseudo-images decreases. An important result is that in the third regime, contrast fluctuations of orders (n, 2) disappear, so these pseudo-images form for any value of the distances between gratings. Any other order disappears. Another interesting result is that a large spectral width produces a change of regime (from the second to the third) for collimated light.

Acknowledgments

This work has been supported by the Ministerio de Ciencia y Tecnología of Spain (contracts no. DPI2001-1238 and DPI2001-1369).

#4362 - $15.00 US Received 13 May 2004; revised 22 May 2004; accepted 25 May 2004
(C) 2004 OSA